Present-day Deformation in the Incipient Strike-slip Basin of the Okavango Delta (Botswana): Impact on the Ecosystem

Olivier Dauteuil, Louis Gaudare, Marc Jolivet, Mickael Murray-Hudson, Piotr Wolski, Kaelo Makati, Moss Edmison

TEKTONIKA

Present-day Deformation in the Incipient Strike-slip Basin of the Okavango Delta (Botswana): Impact on the Ecosystem

Olivier Dauteuil *[1], **Louis Gaudaré** [1], **Marc Jolivet** [1], **Mickael Murray-Hudson** [2], **Piotr Wolski** [3], **Kaelo Makati** [2], **Moss Edmison**[2]

[1]Géosciences-Rennes, UMR 6118, University of Rennes, 35042 Rennes, France | [2]Okavango Research Institute, University of Botswana, Private Bag 285, Maun, Botswana | [3]Climate System Analysis Group, University of Cape Town, Private Bag X3, 7701, Rondebosch, Cape Town, South Africa

Abstract The southward propagation of the East African Rift System inside the Southern African Plateau generates the Okavango Graben, hosting the Okavango Delta, which is one of the largest African endoreic ecosystems associated with an alluvial fan. The deformation and kinematics governing this propagation are still currently being debated, especially whether a strike-slip component is present and whether its impact on the dynamics of ecosystem was ever considered. To go further, we analysed the ground deformation from a network of semi-permanent GNSS stations located inside and around the Okavango Delta. As estimated from previous works, the Okavango Graben is submitted to a right-lateral displacement with highest strain along one border of the graben, where most of the seismicity is located. The inner floor displays a clockwise rotation generating local low intensity compression. This deformation pattern agrees with the asymmetric 3D shape of the basin. The ground subsides with higher rates in the north-east, generating a regional tilt that explains the progressive shift of the annual flood toward the north-east, as described in previous works. This tilting causes some areas to dry up and other areas to become almost permanently flooded. Therefore, we hypothesize that tectonic driving is responsible for the eastward migration of water which could then result in its capture by the Linyanti and Zambezi rivers. The long-term consequence of this deformation is the disappearance of the endorheism of the alluvial fan. This drastic hydrological change will disrupt the ecosystem and impact biodiversity as well as economic resources.

Executive Editor:
Craig Magee
Associate Editor:
Hongdan Deng
Technical Editor:
Mohamed Gouiza

Reviewers:
Daniele Maestrelli
Yanyan Wang

Submitted:
15 April 2024
Accepted:
5 August 2024
Published:
29 October 2024

1 Introduction

The East African Rift System accommodates the continental breakup of the eastern part of the African plate into a set of microplates (*Stamps et al.*, 2008; *Saria et al.*, 2013; *Fernandes et al.*, 2013; *Stamps et al.*, 2021). This breakup propagates southward, generating a set of rift basins often associated with large lakes which are hot spots for biodiversity (*Junk et al.*, 2006; *Mladenov et al.*, 2007; *Ramberg et al.*, 2006; *Moliner Cachazo et al.*, 2023) and have a crucial socio-economic role. Thus, understanding the active deformation in such basins is a key issue both in terms of geodynamic processes and ecosystem dynamics. The opening of the East African Rift System is usually considered as roughly perpendicular to the main fault pattern, either generating a homogeneous subsidence of the basin floor or tilting in the case of asymmetric basins (*Chorowicz*, 2005). However, geodetic studies and field works have described an oblique opening, either during the initial stage of rifting (*Bonini et al.*, 2005; *Corti*, 2009) or at the present time, that can have an impact on basin subsidence. Few works describe the internal deformation in an incipient rift basin formed under a strike-slip context (*Jolivet et al.*, 2013), and none evaluate its impact on the evolution of the ecosystem.

The Okavango Rift System, developing between the Congo craton and the Kalahari craton in northern Botswana (Figure 1), is an ideal object to study the present-day phase of a transtensive strike-slip fault system within the continental crust (*Pastier et al.*, 2017; *Gaudaré et al.*, 2024). The rift hosts the Okavango Delta, an endoreic wetland ecosystem, inscribed as the 1000th UNESCO World Heritage Site. The Delta supports a high concentration of wildlife sustained by an annual flood inundating the swamps. Several geodynamic models describe the Okavango Rift System as a new incipient rift resulting from the propagation of the East African Rift (*Modisi*, 2000; *Kinabo et al.*, 2007; *Saria et al.*,

*✉ olivier.dauteuil@univ-rennes.fr

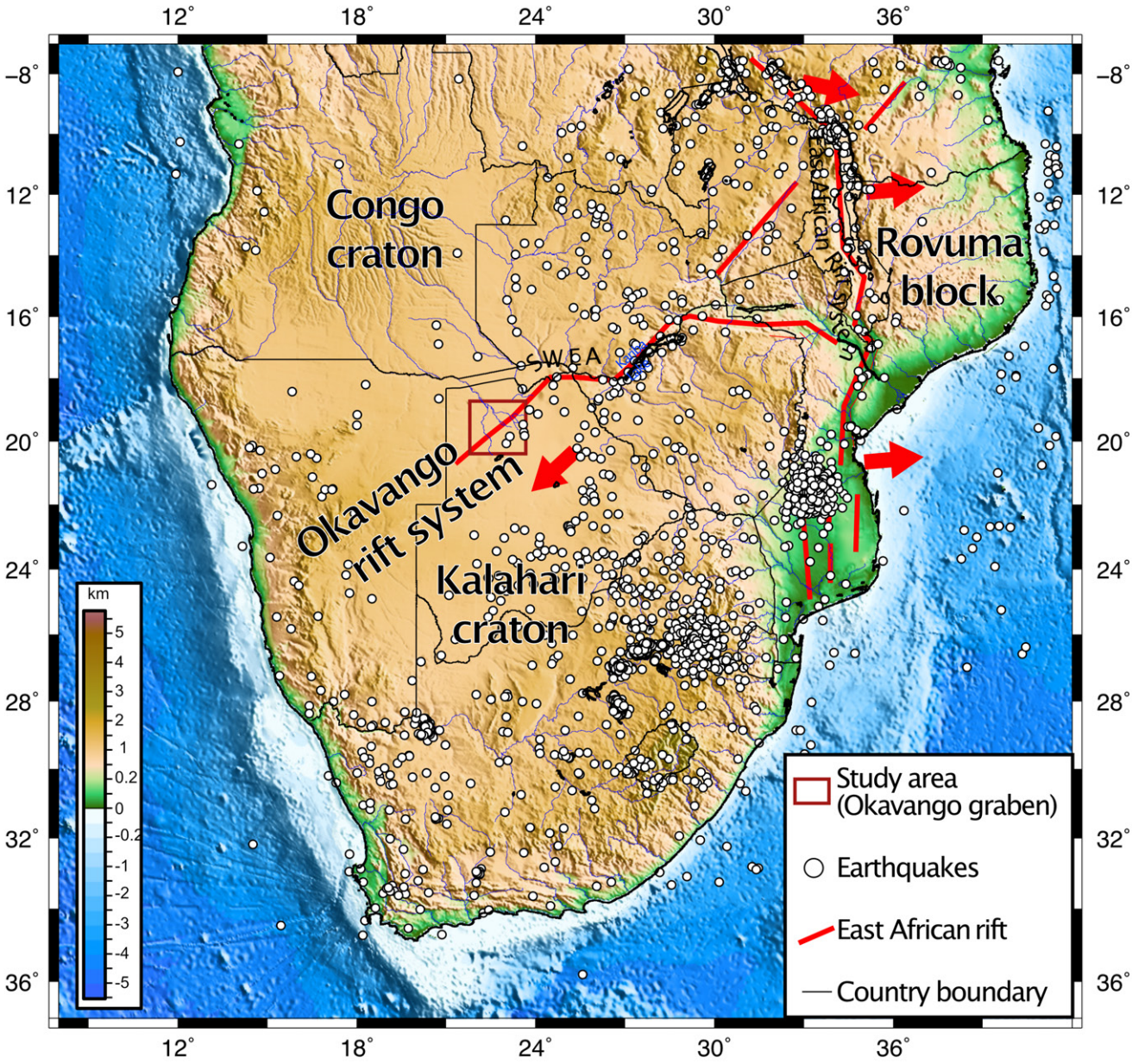

Figure 1 – Location of the Okavango Delta inside the Southern African plateau. The white dots indicate the earthquakes since the year 2000 (USGS database), the red lines demarcate the East African Rift and the red arrows show the regional displacements relative to the Nubian block (*Saria et al.*, 2013; *Pastier et al.*, 2017).

2013; *Yu et al.*, 2017), and assume the opening to be perpendicular to the main trend of the rift, i.e. NW-SE. However, *Pastier et al.* (2017) highlighted that this rift basin forms under strike-slip conditions, based on a regional geodetic study with a differential displacement rate of nearly 1 mm/yr measured between the Kalahari craton to the SE and the Nubian block to the NW. A recent work (*Dauteuil et al.*, 2023) combining the water equivalent thickness using GRACE data (*Landerer and Swenson*, 2012) and GNSS data highlights the impact of regional precipitation on ground deformation. The major rainfall in Angola (> 1000 mm/yr) and consecutive flooding in the Okavango Delta (ca. 11 km^3/yr of flood water) induces vertical loading recorded by both GPS time series and GRACE data. The vertical ground displacement reaches 5 cm in Angola and decreases progressively southward down to 2 cm in Maun (Botswana). The centimetric amplitude of the rainfall-driven periodic signal is larger than the millimetric amplitude expected for geodynamic processes. The cumulation of weak displacements induced by geodynamic processes may impact the hydrological dynamics of the Delta by changing the regional slope or generating scarps modifying the flood migration and, in turn, threatening established ecosystems. To further investigate the ground deformation of the Okavango Graben, we measured the deformation with a regional-scale geodetic network and evaluated the impact of the deformation on the hydrology of this unique ecosystem.

2 Geological Overview

The Okavango Rift System (Figure 2), including the Okavango Graben to the NW and the Makgadikgadi Basin to the SE (*Moore et al.*, 2012; *Gaudaré et al.*, 2024), affects the late Neoproterozoic Damara belt resulting from the collision between the Kalahari and Congo cratons. It recorded different episodes of continental sedimentation that lasted from the Permian to the Early Cretaceous, forming the Karoo supergroup (*Miller*, 2008; *Lovecchio et al.*, 2020). During this period, a Triassic extensional phase generated NE-SW rifts and large volcanic floods occurred during the middle Jurassic (*Jourdan et al.*, 2005). Then, the landscape was intensively weathered during the Late Cretaceous to the Miocene forming thick lateritic profiles that were subsequently eroded, generating a set of palaeo-surfaces shaping the Southern African Plateau (*Bessin et al.*, 2015; *Dauteuil et al.*, 2018). The Late Cenozoic deposits consist of lacustrine, fluviatile and aeolian sediments forming the Kalahari Group, the thickness of which varies from tens of meters to several hundreds of meters (*Thomas and Shaw*, 1990; *Haddon and McCarthy*, 2005; *Wanke et al.*, 2000). During the Pliocene, a major part of the region was covered by a large aeolian dune field that was later locally reworked by palaeo-lakes and rivers as in the Makgadikgadi Basin. During the Plio-Pleistocene, the south-west propagation of the East African Rift System generated the Okavango Graben, shaped by NE-SW faults (*Bufford et al.*, 2012), and a widespread fault system in the Makgadikgadi Basin (*Moore et al.*, 2012) located above the northern side of the Kalahari Craton. The structural relationships between the fault pattern of the Makgadikgadi Basin, Okavango Graben and Kariba Rift to the east result in a progressive propagation driven by the displacement and rotation of the San plate (*Daly et al.*, 2020; *Wedmore et al.*, 2021; *Gaudaré et al.*, 2024). This propagation first generated a widespread faulting ranging from the Makgadikgadi Basin to the Okavango Graben that became localized in the Okavango Graben. In the Okavango Rift System, seismic activity is very low with few, low-magnitude events (*McCARTHY*, 2013). Earthquakes are mainly located on the SE side of the graben, at an estimated depth up to 20 km, and are widespread in the Makgadikgadi pan with a magnitude less than 4 (Figure 2). The last large earthquake occurred in April 2017 (Mw 6.4), 100 km south of the southern edge of the pan (*Materna et al.*, 2019), and had an extensional mechanism.

The age of the Okavango Rift System is poorly constrained due to the lack of well-dated direct markers. The oldest described sediments in the Makgadikgadi Basin were estimated to be Miocene in age based on pollen assemblages (*McFarlane and Eckardt*, 2006; *Moore et al.*, 2012; *Podgorski et al.*, 2013). No data are available on the age of the oldest sediments inside the Okavango Graben because the boreholes are not deep enough. The youngest sediments affected by the faults are in the Alab dune field located to the west of the graben, which covers NW Botswana and NE Namibia, and for which a Late Pliocene to Early Pleistocene age was proposed (*Miller*, 2008; *Moore et al.*, 2012). The Gumare Fault to the NW (*McFarlane and Eckardt*, 2006) and the Thamalakane Fault to the SE offset the dunes of the major Alab dune field. (*Miller*, 2008) and *Moore et al.* (2012) proposed that this dune field was very active during the Late Pliocene-Early Pleistocene (ca. 4 to 2 Ma). Inside the graben, the dunes have been reworked by rivers and covered by the deposits from the Deception palaeo-lake dated older than 500 kyr, probably Early Pleistocene in age (*McFarlane and Segadika*, 2001; *Moore et al.*, 2012). Yet, younger ages of 120 kyr, 40 kyr and 27 kyr have been proposed for the initiation of the graben using thermoluminescence and OSL techniques and ages of 100-300 kyr based on archaeological evidence (*Moore et al.*, 2012). However, these younger ages correspond to climatic changes recorded by some diagenetic processes, or to changes in sediment supply, or to changes in the water level of the Makgadikgadi Basin (*Ringrose et al.*, 2005; *Huntsman-Mapila et al.*, 2006; *Burrough et al.*, 2007). Based on these indirect data, the initiation of the graben is assumed to have occurred during the Upper Pleistocene, filled by a palaeo-lake until 500 kyr, which was then replaced by an alluvial fan (*Moore et al.*, 2012).

Presently, the Okavango Delta is an alluvial fan forming a huge swamp with thousands of islands separated by a complex network of channels flowing southward (*McCARTHY*, 2013). This swamp is flooded yearly by water coming from the Angolan mountains and migrating toward the southeast over a five-month period. Every year, roughly 11 km^3 (i.e. 11.109 t) of water inundates the swamp and disappears via evapotranspiration. Only 4% flows outside the delta through two small rivers (*Bauer et al.*, 2004; *Gumbricht et al.*, 2004; *McCarthy*, 2006).

3 Displacement Processing and Strain Calculation

3.1 GNSS Processing

The deformation field affecting the Okavango Graben was estimated using a network of seven semi-permanent GPS stations located inside and around the Delta and a permanent station located at the Okavango Research Institute in Maun, Botswana (Figure 2). The sites were installed in 2010 and visited in 2012, 2014, 2022 and 2023. Stations are installed inside schools, in a lodge garden and close to a park gate so that the stations are in safe places (Table 1). The daily position of each station was recorded using geodetic-type dual-frequency GPS receivers during a minimum period of 24 hours, equipped with geodetic antennas. Positions were calculated

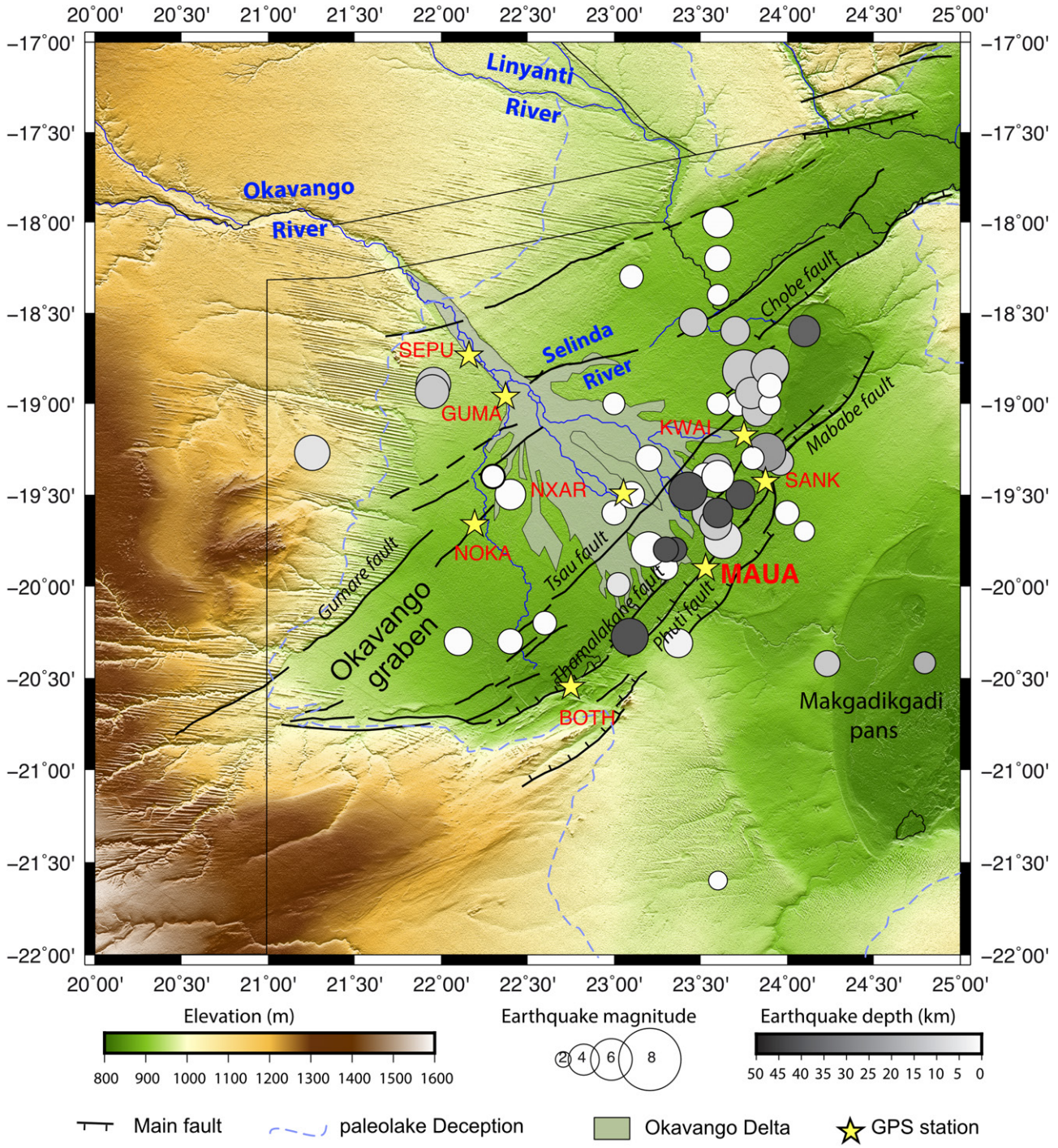

Figure 2 – Structural map of the Okavango Graben with the seismicity (grey circles) plotted against the topography (COPERNICUS DEM, European Space Agency, 2021). The yellow stars with red labels represent the geodetic network used in this study. The thick black lines are the faults and the thin lines are the national boundaries. The MAUA station is used to calculate the relative displacements. The dashed blue line displays the shoreline of the palaeo-lakes Deception (drawing from *Moore et al.*, 2012; *Gaudaré et al.*, 2024).

using the Precise Point Positioning (PPP) technique with the RTKLib package (*Takasu*, 2010). Precise ephemerides and clock corrections were included in the processing. The elevation cutoff angle was set to 10°. The zenithal tropospheric gradient estimation and Ocean Loading Model were integrated in the data processing. The permanent station located in Maun (MAUA), belonging to the AfricaArray network, was used to compare this study to previous works (*Saria et al.*, 2013; *Pastier et al.*, 2017).

The study area undergoes a significant annual regional deformation induced by the regional-scale rainfall cycle which generates vertical displacements up to 3 cm (*Pastier et al.*, 2017; *Dauteuil et al.*, 2023). Thus, variations in the absolute positions of the stations are the result of hydrological and geodynamic processes. As this work focuses on geodynamic deformation, displacements induced by

Table 1 – location of the GNSS sites (see location in Figure 2)

Site NAME	Longitude	Latitude	Elevation (m)	Location	Time coverage (hours)				
					2010	2012	2014	2022	2023
BOTH	22.7501	-20.5479	964.7	Botlhatlogo Primary School	48	112	25	22	25
GUMA	22.3727	-18.9622	992.9	Guma Lagoon Camp	13.75	41	8	16	16
KWAI	23.7503	-19.1744	951.5	North Gate of Moremi park, close to Khwai village	18	15	23	24	18
MAUA	23.5283	-19.9022	960.8	Okavango Research Institute at Maun	daily	daily	daily	daily	daily
NOKA	22.1942	-19.6620	972.8	Nokaneng Primary school	42	47	25	16	24
NXAR	23.1791	-19.5480	963.1	Nxaraga island, inside the Delta	daily	8	daily	No	daily
SANK	23.8743	-19.4289	957.8	Sankuyo school	25	24	24	11	25
SEPU	22.1612	-18.7355	1011.8	Sepopa school	24	10	24	24	24

regional rainfall needs to be removed. To remove the hydrological component on the displacements, we used the daily positions of the permanent MAUA station (Figure 2) as the reference for ground deformation induced by hydrological cycles and estimated the positions of the other semi-permanent stations relatively to MAUA. For this, we adjusted the positions of MAUA to 0, and calculated the relative positions of each station every day, by subtracting the displacements of MAUA to the other stations. *Dauteuil et al.* (2023) did not highlight a significant time offset of the variations in the ground deformation between the north and south of the Okavango graben that could be due to the flood migration, thus the corrections relative to MAUA can be applied everywhere.

We estimated the field displacement between four intervals starting in 2010, the first year the network was installed: 2010-2012, 2010-2014, 2010-2022, and 2010-2023. Note that no data were recorded in 2022 at the NXAR station because the receiver was out of order. The 2010-2023-time interval provides a ten year trend of the ground deformation. For each time step, we calculated the absolute displacements and the displacements relative to MAUA, which was assumed to be a fixed reference. The values of the displacement amplitudes and rates are provided in the supplementary material.

3.2 The Strain Field

To evaluate the ground deformation, we estimated the strain inside the graben from the geodetic network that provides only punctual displacements. The deformation is the gradient of the displacement field; i.e. a change in the shape of a network can be converted into rotational, translation and dilatation components, thus defining the strain field (*Allmendinger et al.*, 2012; *Cardozo and Allmendinger*, 2009; *Ramsay and Huber*, 1983; *Wu et al.*, 2011). We computed the strain with the SSPX software (*Cardozo and Allmendinger*, 2009). The strain field was calculated from the 3D vectors of the displacements of the GNSS network nodes organized into a set of triangles, the summits of which are the GNSS stations. A flat triangle was removed because it covers the whole width of the graben, crossing the faults. We extracted two pertinent parameters of the strain: the horizontal rotational component to map the rotation distribution inside the graben and the maximum of the 3D shear strain.

4 Recent Ground Displacements

4.1 Displacement Field in the Absolute Framework

In the absolute reference, most of the points move toward the NNE (from N011° to N070°) at rates ranging from 6 mm/yr to 70.3 ± 10 mm/yr (Figure 3, Table SI-1 in Supporting Information). The amount of displacement increases with time revealing an incremental accumulation, while the direction remains roughly constant. Note that only the BOTH station slightly moves northward. The displacement direction of the stations between each time laps slightly varies, except for MAUA which varies at a slightly higher rate. This NNE-NE azimuth trend is consistent with the direction of the Nubian plate previously estimated by *Saria et al.* (2013) and *Pastier et al.* (2017). The absolute vertical rates range from -20 mm/yr to 11 mm/yr with changing subsiding and uplifting domains for each period (Figure 3, Table SI-1 in Supporting Information). Most of the time, the MAUA site moves upward and the NE domain mostly subsides or moves upward at slower rates than the SW domain.

4.2 Inner Displacement Field

The horizontal displacements relative to MAUA display a wide range of directions Table SI-2 in Supporting Information). Most of the points migrate from the NE to ESE or toward the NW, with rates ranging from 3 to 66 mm/yr, consistent with the right-lateral strike-slip context of the Okavango Graben (Figure 4, Table SI-2 in Supporting Information). The BOTH and SANK stations on the south-eastern side of the graben have weak horizontal displacements relative to MAUA, slightly trending toward the northeast, indicating that these three stations move at a similar rate because they are located on the same tectonic block of the southeast border of the graben, limited by the Thamalakane and Phuti faults. The displacement

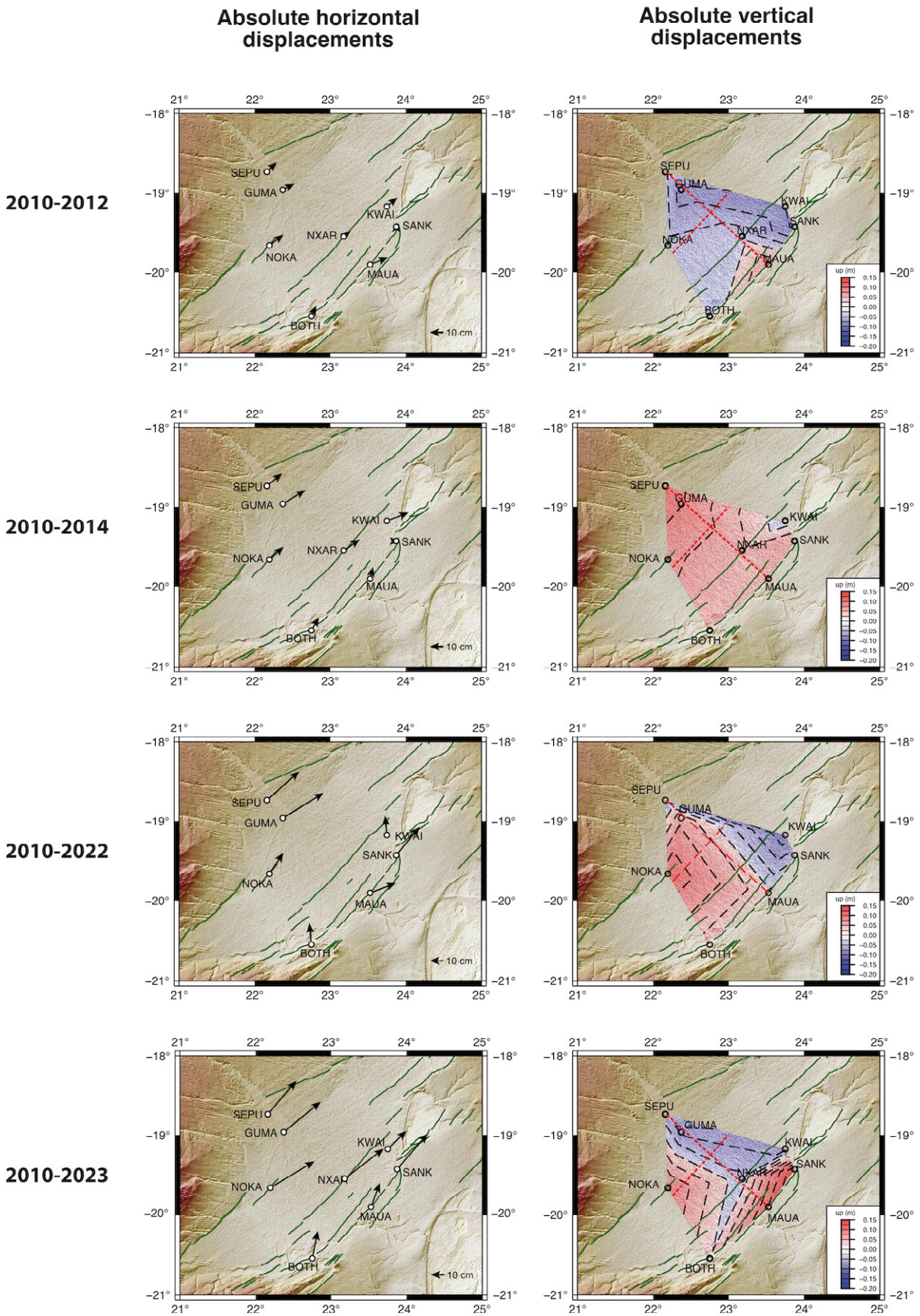

Figure 3 – Maps of the horizontal (left) and vertical (right) displacements from 2010 with their positions in the absolute reference. **a)** 2012, **b)** 2014, **c)** 2022, **d)** 2023. The green lines represent the main faults (this work), and the black arrows are the horizontal displacement vectors. The red dashed lines locate the subsidence profiles in Figure 5. The vertical displacements are interpolated with the Triangulated Irregular Network (TIN) method: blue = downward, red = upward. The dashed lines are the displacement contours every 2.5 cm.

rates roughly increase toward the NW. Stations KWAI and SANK display wider ranges in azimuth and rate displacements that could be due to their location at the junction between two faults that change in direction (green lines in Figures 2 and 4).

Maps of the relative vertical displacements display domains in subsidence and domains in uplift with values ranging from -64.1 mm/yr to 16.7 mm/yr. The subsidence rates are higher than the uplift rates Table SI-1 in Supporting Information). Except for the two first years (map of 2012), the uplifting domain (in red in Figure 4) becomes narrower over time compared to the domain in subsidence. The north-western border of the graben displays both upward and downward displacements. The SANK station displays upward or downward motions. The two subsidence profiles (Figure 5) better display this distribution of the vertical displacements. On the NW-SE profile, the subsidence is higher toward the NW and ceases 140 km away from the NW, corresponding approximately to the Thamalakane fault. This change in subsidence slope is not well constrained because the interpolation was calculated with a limited number of points. The SW-NE profile shows a general tilting toward the NE.

4.3 The Decadal Strain

To evaluate the long trend evolution of the deformation of the graben, we estimated the strain by comparing the changes in the network shape between 2010 and 2023. The two selected strain field components (rotation and maximum shear strain) provide pertinent additional information about ground deformation inside the graben (Figure 6). The highest shear strain is located along the south-eastern side of the graben where most faults are located (Thamalaklane fault, Phuti fault). The shear strain is low along the north-western border. The lowest maximum shear strain values are inside a NE-SW corridor in the middle part of the graben, i.e. far away from the known or inferred faults. There is a fall in the shear strain in approximately the middle part of the graben where some faults are inferred, like the Tsau fault (Figure 2). The rotational component of the strain displays a clockwise rotation in all the triangles of the network, except the northern one located between the SEPU, NOKA and GUMA sites. This latter one partially crosses the Gumare fault (GF on the map shown in Figure 6). The amount of rotation decreases roughly from the SE toward the NW, consistent with the shear strain distribution. The two joined triangles display a main difference in amount of rotation, south of the survey area: i.e. triangle (NOKA, BOTH, NXAR) with a low value and triangle (NXAR, MAUA, BOTH) with the highest value. The difference in rotation can generate a localized shortening inside the graben; however, this is difficult to determine because the small number of stations means that a detailed strain analysis cannot be performed.

5 Discussion

5.1 Deformation Pattern and Basin Structure

The local GNSS study shows that the Okavango Graben is submitted to a right-lateral strike-slip deformation, confirming a previous regional-scale geodesic analysis (*Pastier et al.*, 2017) and certain geophysical studies proposing a right-lateral offset of 1.5 km of a large Mesozoic dyke swarm in the Delta basement (*Campbell*, 2005; *Chisenga et al.*, 2020; *Schmidt et al.*, 2023). The highest shear strain is located along the south-eastern border of the basin (Figure 6), with increasing intensities close to the BOTH station to the south, where the fault scarp of the graben is the highest (up to 50 m), confining Lake Ngami. This strain distribution also fits with the earthquake pattern, showing a higher frequency along the south-eastern side of the graben than in the inside or along the north-western side (Figure 2). Unfortunately, no focal mechanism is available.

This deformation pattern observed in map view is consistent with the 3D structure of the basin. *Kinabo et al.* (2007) and *Bufford et al.* (2012) described an asymmetric graben with more sediments in the southern part (> 400 m) than on the northern side (tens of meters) forming a sedimentary wedge (Figure 7). (*McFarlane and Eckardt*, 2006) estimated that the Gumare fault accommodates a vertical throw of 25 m, north of the graben. To the south, the vertical throws along the Thamalakane fault and Phuty fault are unknown. However, the accumulation of some hundred meters of sediment imposes a vertical throw of at least the same value. This asymmetric fault pattern is compatible with the geodesic results that show extension on the southern border and a clockwise rotation inside the graben and along the northern side of the graben. The SE border displays a high transtensive deformation associated with normal faults, allowing for the accumulation of thick sediment deposits, whereas the opposite NW border is limited by a steep strike-slip fault with a small vertical throw and low sediment accumulation (total sediment thickness < 30 m) (Figure 7). Note that there are more earthquakes along the south-east border than along the other opposite one. The inner part of the graben accommodates this difference in structural pattern with a clockwise rotation, a decrease in strain northward and probably by unmapped faults with weak activities (Figure 2). Relative to MAUA, the deformation rate inside the graben is roughly constant (Figure 7) except for station KWAI (discussed below), which could contradict the seismicity distribution that is mainly located along the southwest border (Figure 2). To take these observations into account, we suggest that the NW border of the graben is submitted to a slow aseismic creeping whereas the SE border is affected by discontinuous deformation. The KWAI station is located in the northwest part of the study area, at the junction between two faults that trend north-south in

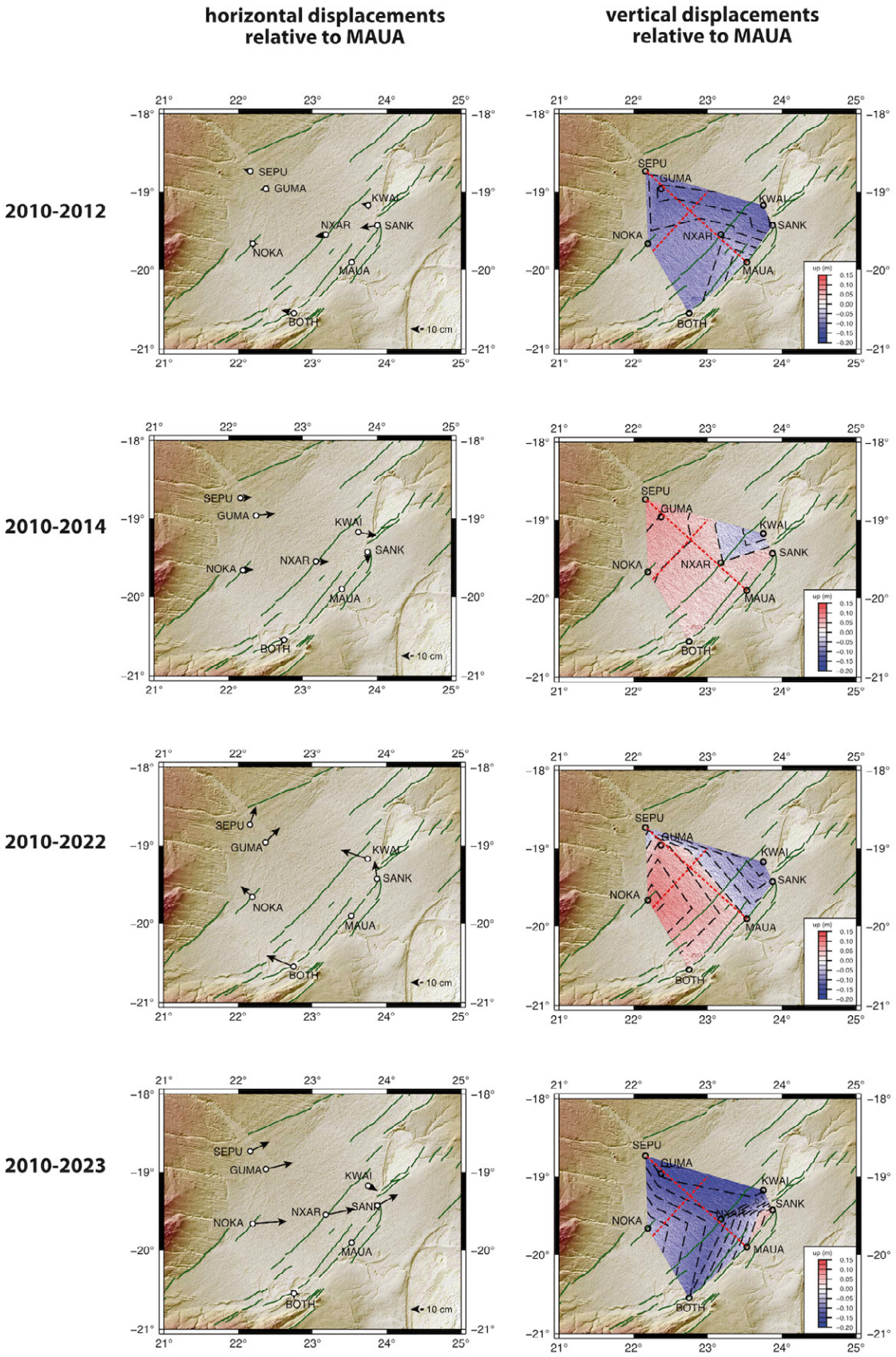

Figure 4 – Maps of the horizontal and vertical displacements from 2010 with positions relative the MAUA station. **a)** 2012, **b)** 2014, **c)** 2022, **d)** 2023. The green lines represent the main faults (this work), and the black arrows show the horizontal displacement vectors. The red dashed lines provide the location of the subsidence profiles in Figure 5. The vertical displacements are interpolated using the TIN method: blue = downward, red = upward. The dashed lines are the displacement contours every 2.5 cm.

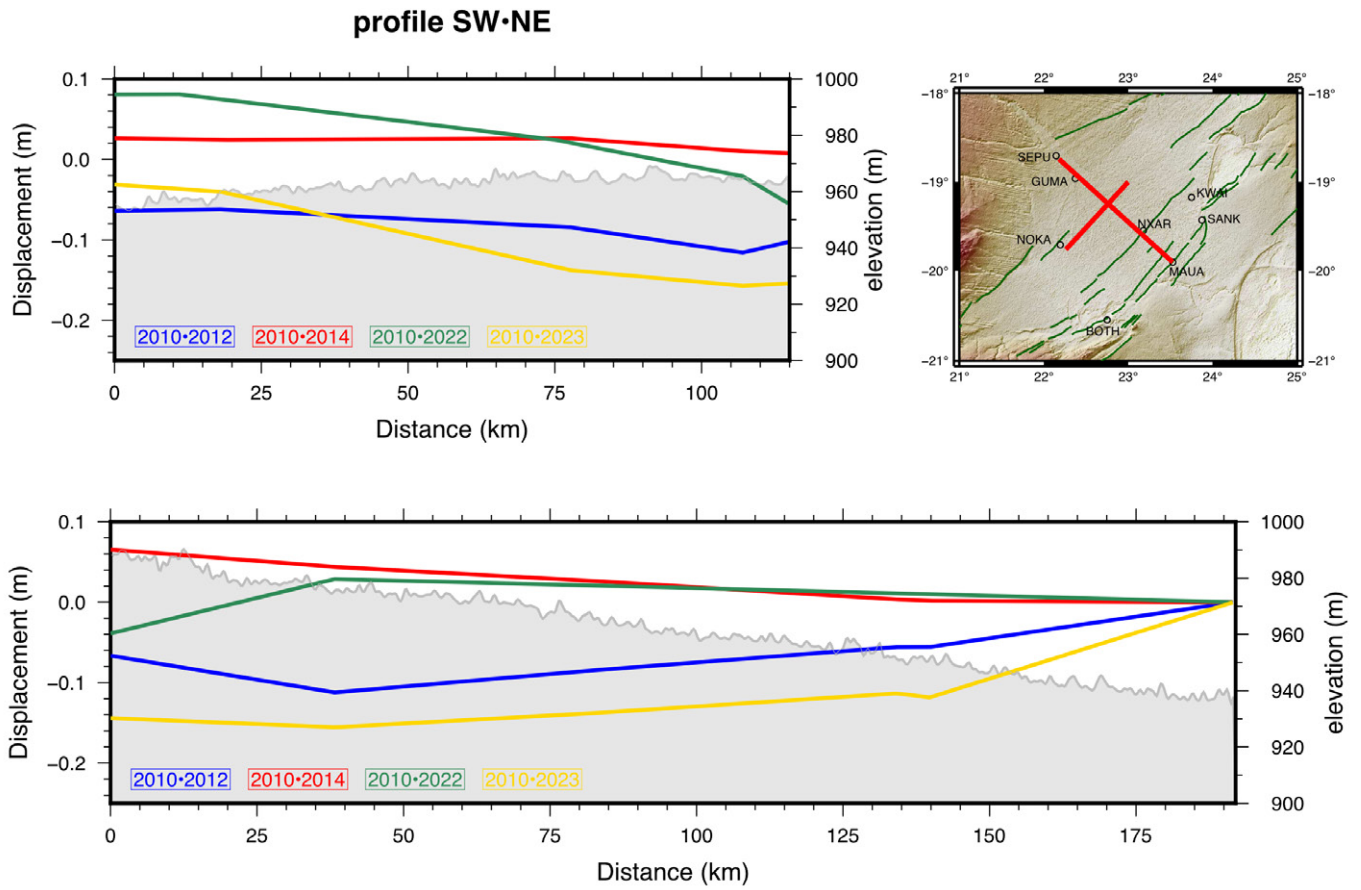

Figure 5 – Profiles of the vertical displacements during the different periods. Upper right: location of the profiles, upper left: NW-SE profile, lower: SW-NE profile. The light grey area displays the topography along the profile. These subsidence curves show that the graben ground tilts toward the NE and SE. Note the slope break along the NW-SE profile at a distance of 140 km from the NW that is correlated to the Thamalakane fault.

this area while they are oriented NE-SW southward. This structural setting of the faults thus blocks the lateral displacement, thereby generating a higher subsidence.

The creep behaviour of a strike-slip fault was previously described along a lateral-shearing system (*Cakir et al.*, 2005; *Titus*, 2006). Several hypotheses can be put forward to explain these differences in kinematic behaviour between the two borders of the graben: a change in the lithology and in particular the grain size of the basement (*Gratier et al.*, 2013), the roughness of the fault plane (*Dyer et al.*, 2012) and fluid circulation (*Brantut et al.*, 2013). The first two hypotheses can be retained because the Okavango Graben is located at the transition between various blocks of the Neoproterozoic Damara belt and a remnant block of a Mesoproterozoic orogen, whose trend drove the border faults of the graben. It corresponds to the reactivation of the Damara vertical structures generated during the collision between the Kalahari and Congo cratons. Based on present-day knowledge, the fluid circulation hypothesis can be rejected because no such deep circulation has been evidenced by previous works focused on seismic activity in the Delta (*McCarthy*, 1993; *Gumbricht et al.*, 2001; *Pastier*, 2018).

5.2 Ground Deformation at the Scale of the Graben

Two processes are involved in the ground deformation of the Okavango Delta: regional geodynamics and water loading induced by climatic cycles (*Pastier et al.*, 2017; *Dauteuil et al.*, 2023). Our study focuses only on the geodynamic process.

Our deformation study shows that the ground of the Okavango Graben subsides with a tilt toward the northeast with a high rate (cm/yr). Subsidence is also high on the NW side of the graben, which is not consistent with the high sediment thickness located to the SE (Figure 7). We propose that this might be due to a recent change in the deformation distribution. In an initial step, the graben initiated with a main faulted zone at SE, forming a half-graben accumulating a large amount of sediment on this side. Then a very recent change in the geodynamic conditions generates a shift in the subsidence location to the NW. This change is too recent to be well recorded in the sediment accumulation. However, we can note that the domain located at the exit of the panhandle is always under water, regardless of the flood intensity, and displays less emerged lands compared to the other domains of the Okavango swamp. These two observations fit with a domain where the bottom

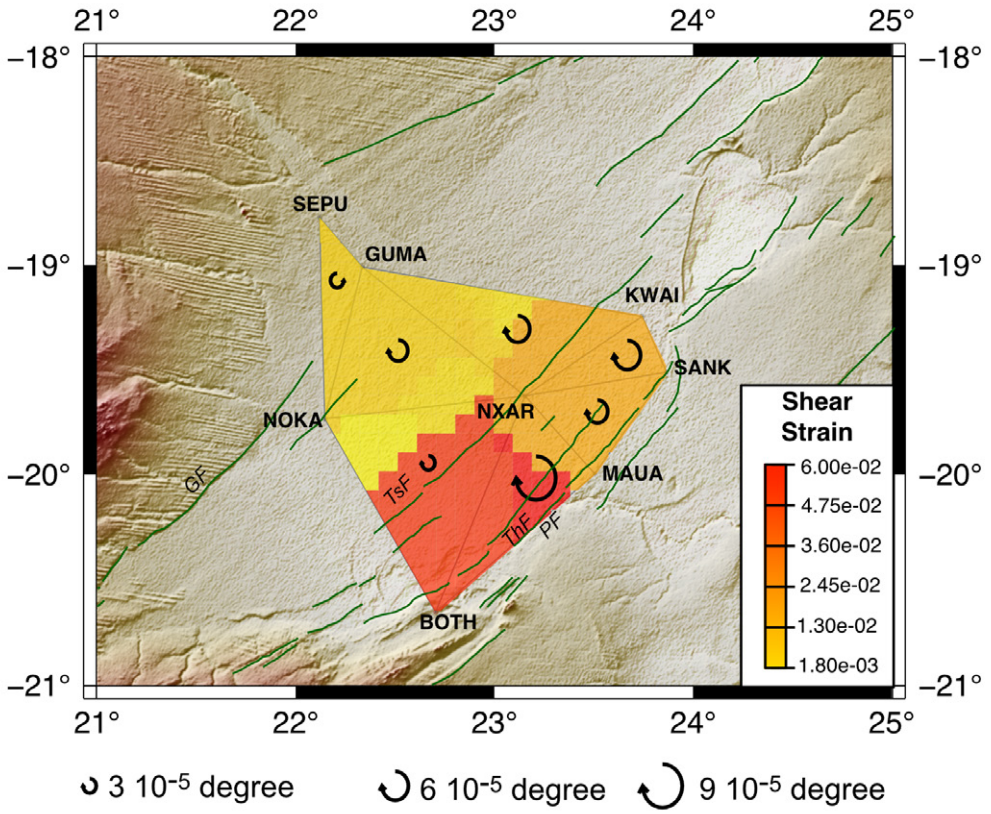

Figure 6 – Strain analysis deduced from the displacements of the stations. The coloured triangles correspond to the shear strain, the black rounded arrows indicate a rotation, and the green lines show the faults (this work). Note that there is a change in the extension direction from the SE to the N and the highest dilation is found to the north. GF: Gumare fault, TsF: Tsau fault, ThF: Thamalakane fault, PF: Phuti fault.

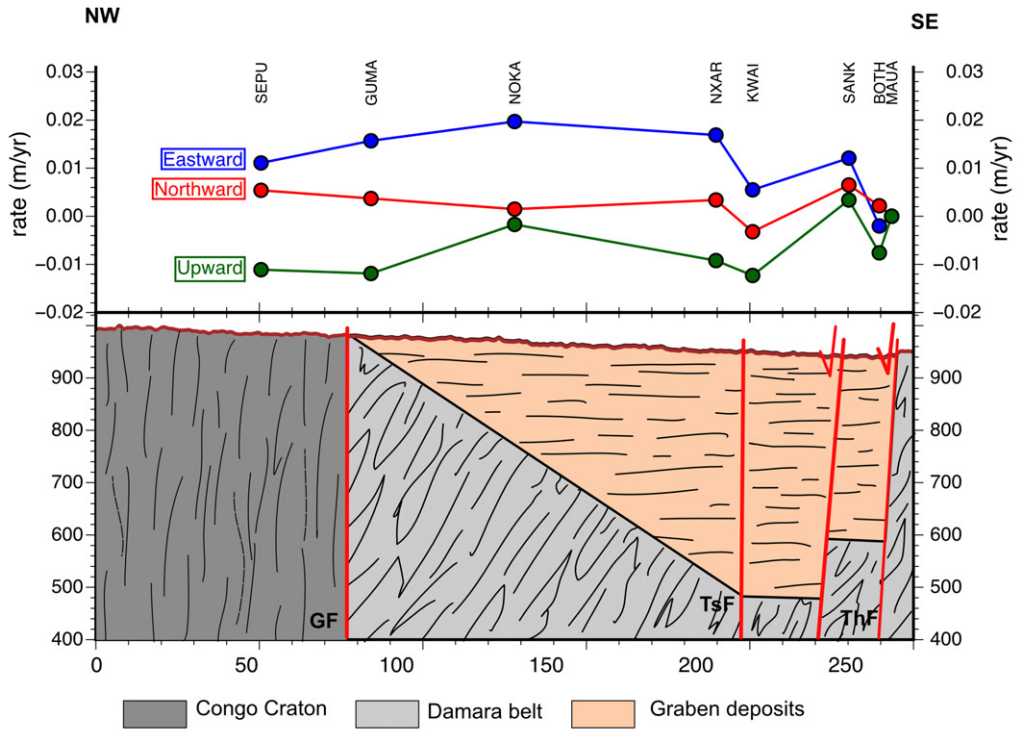

Figure 7 – Synthetic section showing the displacements inside the Okavango Graben projected along a NW-SE direction. The upper plot shows the eastward (in blue), northward (in red) and upward (in green) components of the displacement. The lower plot displays a simplified geological section compiled from previous works (*Key and Ayres*, 2000; *Bufford et al.*, 2012; *Gaudaré et al.*, 2024) and field observations (this study). GF: Gumare fault, TsF: Tsau fault, TF: Thamalakane fault.

sinks, providing permanent water storage and silting up the previously emerged lands.

This deformation should impact the evolution of the Okavango Delta hosted by the graben. In addition to the geodynamic context, the dynamics of the ecosystem of the Okavango Delta are driven by the annual flooding that inundates an area ranging from 3500 km^2 to 8500 km^2. The results of this work raise the question of the impact of this deformation on water migration during annual floods. Two scenarios may explain a shift of the water propagation toward a new direction: a change in the regional slope or a blockage of water in a restricted area due to fault activity, sediment accumulation or vegetation. Figure 8 compares the subsidence distribution to the frequency of flooding over a 15 year period (*Gumbricht et al.*, 2004): the highly subsiding areas (dark blue in Figure 8) are always inundated (more than 80% of time during 15 years); while the areas with low subsidence or in uplift (in light blue or red) are more rarely inundated (less than 20% of time during 15 years). *McCarthy et al.* (2003) also described a shift of the inundated areas toward the north-east from 1985 to 2000. Some field observations report the abandonment of channels in the western part of the Delta, no longer providing water for Lake Ngami since the 1920s (*Burrough et al.*, 2007; *Wolski and Murray-Hudson*, 2008). Previous studies have ruled out the blockage of these channels by vegetation, instead suggesting that tectonic subsidence has had an effect (*McCarthy et al.*, 1993; *Ellery and McCarthy*, 1998). In addition to this regional impact of ground deformation on water flow, a local change in slope induced by a fault can block or unblock a tributary. This tectonic control can be inferred in the block limited by the Thamalakhane and Phuti faults north of Maun: this area is inundated by recent floods, while the palaeo-lake that covered the Okavango region never deposited sediments at that site (*Gumbricht et al.*, 2001). In the middle of the Delta, the highly flooded area seems limited to the southeast by an inferred fault (grey line in Figure 8). Clearly, tectonics drives an important part of the flood distribution.

The second effect of ground deformation concerns sedimentary transfers. In general, an alluvial fan accumulates sediments that fans out from a localized source of sediments. At the regional scale, this accumulation forms a geomorphic feature shaped like a section of a shallow cone, with its apex at the source of the sediments. In the case of the Okavango Delta, the panhandle is the sediment input area that concentrates sediment (mainly sand) coming from the Angolan mountains. Inside the Delta, sediments are spread through a complicated set of channels mainly driven by the regional slope, i.e. toward the south-east. There is also an inner redistribution of sediment with domains in erosion that provide material to other domains. Therefore, a change in slope may modify sediment pathways: an increase in slope focuses and increases sediment fluxes and erosion in the slope direction, while a local (fault for instance) and regional inversion (reverse tilting) in the slope blocks sediment transfers. Figure 9 displays two synthetic NE-SW swath topographic profiles extracted from a 5 km-wide band considering the surface of the Deception palaeo-lake (Figure 2) which covered the whole system (*Moore et al.*, 2012) as the base of the recent alluvial fan (*Ringrose et al.*, 2008; *Podgorski et al.*, 2013, 2017). The bottom of the alluvial displays a gentle slope (1.4‰) toward the NE of the NW profile whereas the SE profile has no significant slope (Figure 9). This independent geomorphic observation is consistent with the regional tilt resulting from the GNSS study, reasonably assuming that the palaeo-surface was initially horizontal. The two topographic profiles show that the top of the Okavango alluvial fan has an asymmetric shape that is thicker on the north-eastern side, indicating that sediment fanning leads to higher sediment accumulation on the north-eastern side of the fan. This is consistent with a north-eastward tilt of the palaeo-surface of Lake Deception. The topographic profile trending NW-SE in Figure 5 displays a regular slope toward the southeast, slightly disturbed by channels.

5.3 Impact on the Future Dynamics of the Ecosystem: Toward Exorheism?

The contribution of the tectonic deformation to the wetland dynamics is still being debated (*Milzow et al.*, 2009). However, our results highlight how deformation drives flood propagation and sediment transfer at the local and regional scale. Even if the deformation is significant, it is overprinted by the sediment supply that masks the fault scarps inside the inner part of the graben. However, the consequences of the regional tilting toward the north-east are described. It favours the flood migration toward the north-east and water accumulation to the east of Chief's Island, which is almost always inundated (*Gumbricht et al.*, 2004; *Murray-Hudson et al.*, 2006; *Wolski et al.*, 2006; *Milzow and Kinzelbach*, 2010; *Wolski et al.*, 2017).

The Selinda River located in the north of the Delta (Figures 2 and 10) flows eastward and is intermittently connected to the Linyanti Delta (*Gumbricht et al.*, 2004) that is fed by the Linyanti River coming from the Angolan mountains to the north. The connection between the Linyanti and Okavango drainages occurs during years with large rainfall in Angola (*Shaw*, 1984; *Mendelsohn et al.*, 2010). The Selinda River displays numerous meanders due to the flat topography: the topographic profile along the river (Figure 10b) displays a very gentle mean slope of 0.0085° with two small knickpoints limiting domains with different slopes. The profile has a slope of 0.0087° until the first knickpoint (kp1 in Figure 10b) at 70 km which limits a river segment with a slope of 0.0021°. The second knickpoint (kp2 in Figure 10b) at 90 km separates a segment with a slope of 0.0024°. Then, the profile has a slope of 0.001° and

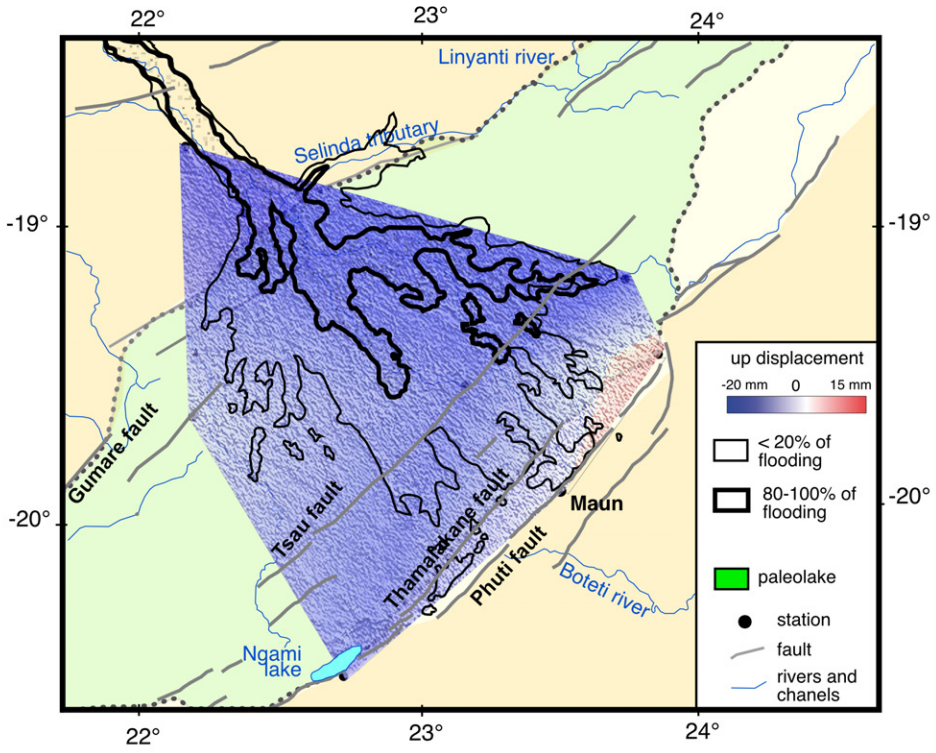

Figure 8 – Flooding frequency over a 15-year period (*Gumbricht et al.*, 2004) compared to the subsidence from the GNSS survey (this study). The domain with a thick black line corresponds to areas that were flooded by more than 80% over a 15-year period, and the domain indicated by a thin line shows areas that were flooded by more than 20% over a 15-year period. The blue-red coloured zone shows the subsidence (see Figure 4). The light green area corresponds to the palaeo-lake that covered the Okavango area (*McCARTHY*, 2013), and the grey lines indicate the faults. Note that the areas with a high frequency of flooding fit with the highest subsiding area, whereas the domains with low subsidence are associated with the lowest flooded domains.

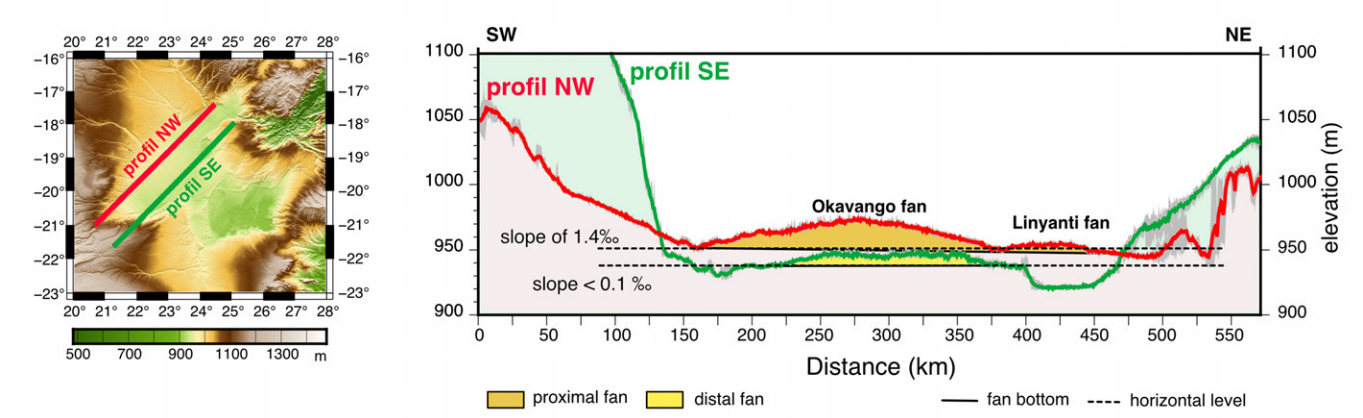

Figure 9 – NW-SE topographic profiles across the Okavango Rift System displaying cross-sections of the alluvial fans. The profiles in red and green are swath profiles compiled from 10 profiles, each 200 m apart, with one point every 100 m, the grey envelops correspond to the unitary profiles. The base of the fans was estimated from the surface of palaeo-Lake Deception (*Moore et al.*, 2012). The palaeosurface was flat when formed and is now tilted toward the NE by 1.4‰.

progressively ends until a normal fault that limits the Linyanti Delta. Just west of knickpoint kp1, a slight decrease in slope that could become reverse (unfortunately the DEM is not accurate enough to determine this) might slow down the water propagation or stack the water when the discharge levels are lower. However, the upstream retreat of the knickpoint will remove the water storing place, allowing for a drainage connection. The knickpoint retreat can be sped up by the increase in regional slope described in this work. The change in slope accelerates the water flow and, by consequence, erosion. Thus, all the conditions are in place for a connection, but it is impossible to predict when this may occur (Figure 10a). If the Selinda River were to capture the Okavango River, this would suppress the endorheic state of the Okavango Delta because the Selinda River is connected to the Zambezi River which flows into the Ocean Indian in Mozambique (Figure 10c). This capture would drastically modify

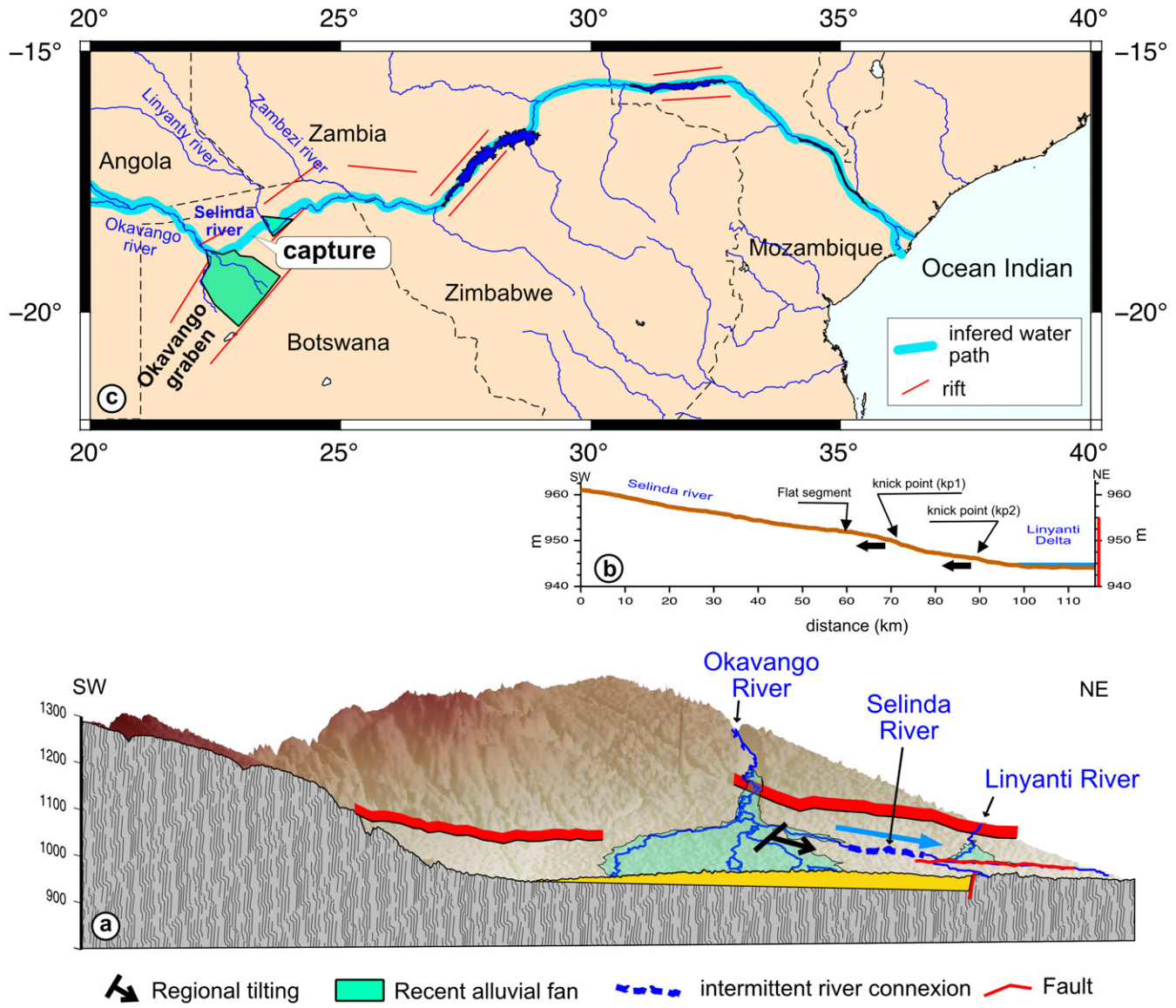

Figure 10 – The capture the Okavango River. **A)** 3D block diagram with a SW-NE slice in the middle of the Okavango Rift System. The thick red lines show the faults on the NW side of the graben, the black arrow shows the tilt of the ground and the light blue line indicates the intermittent connection between the Okavango and Linyanti drainages associated with the Linyanti River. **B)** Topographic profile along the Selinda River displaying the small slopes and knick points (kp1 and kp2). The black arrows indicate the knick point retreats, and the red line shows a normal fault. **C)** General map showing the probable water path (light blue) when the Selinda River will capture the Okavango River.

the hydrological context of the Okavango Delta, which would then become an exoreic ecosystem. This change would generate a drastic reduction in the water flux downstream of the Delta, inducing strong impacts on the biodiversity and economy of Botswana, which is driven by tourism linked to biodiversity. It is impossible to estimate the timing of this scenario, but it could be possibly tens of years when looking at the evolution over the last 50 years. Furthermore, this scenario does not integrate global climate changes, the consequences of which are difficult to assess at present time.

6 Conclusion

The dynamics of an endoreic geosystem result in a coupling between water supply, sediment transport, climate and ground deformation. This study i) estimates the ground deformation affecting the Okavango Delta over the last 10 years, ii) integrates the results in older observations and iii) tries to estimate its impacts for a future evolution. In our study area, two main processes drive ground deformation: variations in the water loading induced by large scale rainfalls and regional geodynamics due to the propagation of the SW branch of the East African Rift since the Plio-Pleistocene. As the yearly effect of the water loading has already been investigated, we focused on the influence of tectonic

processes on ground deformation. The geodynamic context generates an asymmetric strike-slip basin at the crustal scale with a heterogeneous strain field. The strain is higher on the south-eastern side of the graben and displays a clockwise rotation inside the graben with a higher subsidence to the north-east. The distribution of the subsidence impacts the flood distribution by drying domains located to the south-west and by more frequently inundating the north-eastern part of the Delta. If this trend continues, it would drastically change the propagation of water in this region by shifting from an intermittent connection to a permanent connexion between the Okavango Delta and the Linyanti Delta to the east, due to the capture of the Selinda River by the Linyanti and Zambezi systems. The future transition from an endoreic to an exoreic ecosystem would impact the biodiversity and human activities of the Okavango Delta and must be considered in the regional management.

Acknowledgements

This work was funded by the University of Rennes (Scientific Challenges program) and by the CNRS-INSU (Tellus-Rift and SYSTER programs). It is a part of the GDR-CNRS "Rift" program. The GNSS receivers were lent to the Technician Division of the INSU/CNRS (Research Infrastructure GPSMOB). The staff at the Okavango Research Institute were of great help with the fieldwork. We would like to thank the managers of the Botlhatlogo, Nokaneng, Sankuyo and Sepopa schools and the manager of Guma lodge who allowed us to install GPS inside their schools and who provided us with accommodation over a period of several days. Last but not least, we are particularly thankful for the comments and suggestions made by the two reviewers, Dr Hongdan Deng and Dr Yanyan Wang. This work was carried out within the framework of research permit ENT8/36/4L(83) that was kindly provided by the Ministry of Environment, Natural Resources Conservation and Tourism. The GNSS data are available on the OpenScienceFramework website (https://osf.io/czt3a/)

Author contributions

Olivier Dauteuil: project manager, manuscript writing. **Louis Gaudaré**: GNSS processing, data manager. **Marc Jolivet**: CoPi of the project, manuscript writing. **Piotr Wolski**: site and data managements. **Kaelo Makati**: field survey and site. **Moss Edmison**: field survey and site management.

Data availability

The GNSS data of the sites under RINEX format are available on the OpenScienceFramework website (https://osf.io/czt3a/). The CLOCK and SP3 files were downloaded from the RGP/IGN website (https://rgp.ign.fr/DONNEES/serveurs.php). The data were processed with RTKLib package (version 2.4.2) downloaded from https://www.rtklib.com. The site locations were determined with PPP-method.

Competing interests

The authors declare no competing interests.

Peer review

This publication was peer-reviewed by Daniele Maestrelli and Yanyan Wang. The full peer-review report can be found here: tektonika.online/index.php/home/article/view/79/108

Copyright notice

References

Allmendinger, R. W., N. Cardozo, and D. M. Fisher (2012), Structural geology algorithms vectors and tensors | Structural geology, tectonics and geodynamics.

Bauer, P., G. Thabeng, F. Stauffer, and W. Kinzelbach (2004), Estimation of the evapotranspiration rate from diurnal groundwater level fluctuations in the Okavango Delta, Botswana, *Journal of hydrology*, *288*(3-4), 344–355, doi: 10.1016/j.jhydrol.2003.10.011.

Bessin, P., F. Guillocheau, C. Robin, J.-M. Schroëtter, and H. Bauer (2015), Planation surfaces of the Armorican Massif (western France):Denudation chronology of a Mesozoic land surface twice exhumed in response to relative crustal movements between Iberia and Eurasia, *Geomorphology (Amsterdam, Netherlands)*, *233*, 75–91, doi: 10.1016/j.geomorph.2014.09.026.

Bonini, M., G. Corti, F. Innocenti, P. Manetti, F. Mazzarini, T. Abebe, and Z. Pecskay (2005), Evolution of the Main Ethiopian Rift in the frame of Afar and Kenya rifts propagation, *Tectonics*, *24*(1), doi: 10.1029/2004TC001680.

Brantut, N., M. J. Heap, P. G. Meredith, and P. Baud (2013), Time-dependent cracking and brittle creep in crustal rocks: A review, *Journal of structural geology*, *52*, 17–43, doi: 10.1016/j.jsg.2013.03.007.

Bufford, K. M., E. Atekwana, M. Abdelsalam, E. Shemang, E. Atekwana, K. Mickus, M. Moidaki, M. Modisi, and L. Molwalefhe (2012), Geometry and faults tectonic activity of the Okavango Rift Zone, Botswana: Evidence from magnetotelluric and electrical resistivity tomography imaging, *Journal of African Earth Sciences*, *65*, 61–71, doi: 10.1016/J.JAFREARSCI.2012.01.004.

Burrough, S. L., D. S. G. Thomas, P. A. Shaw, and R. M. Bailey (2007), Multiphase Quaternary highstands at Lake Ngami, Kalahari, northern Botswana, *Palaeogeography, palaeoclimatology, palaeoecology*, *253*(3-4), 280–299.

Cakir, Z., A. Akoglu, S. Belabbes, S. Ergintav, and M. Meghraoui (2005), Creeping along the Ismetpasa section of the North Anatolian fault (Western Turkey): Rate and extent from InSAR, *Earth and planetary science letters*, *238*(1-2), 225–234, doi: 10.1016/j.epsl.2005.06.044.

Campbell, A. E. (2005), Shelf-geometry response to changes in relative sea level on a mixed carbonate–siliciclastic shelf in the Guyana Basin, *Sedimentary geology*, *175*, 259–275, doi: 10.1016/J.SEDGEO.2004.09.003.

Cardozo, N., and R. W. Allmendinger (2009), SSPX: A program to compute strain from displacement/velocity data, *Computers & geosciences*, *35*(6), 1343–1357, doi: 10.1016/j.cageo.2008.05.008.

Chisenga, C., Y. Jianguo, I. Fadel, M. v. d. Meijde, and E. A. Atekwana (2020), Updated tectonic terrane boundaries of Botswana determined from gravity and aeromagnetic data, *Episodes*, *43*(4), 919–933, doi: 10.18814/epiiugs/2020/020054.

Chorowicz, J. (2005), The East African rift system, *Journal of African Earth Sciences*, *43*(1), 379–410, doi: 10.1016/j.jafrearsci.2005.07.019.

Corti, G. (2009), Continental rift evolution: From rift initiation to incipient break-up in the Main Ethiopian Rift, East Africa, *Earth-science reviews*, *96*(1-2), 1–53, doi: 10.1016/j.earscirev.2009.06.005.

Daly, M., P. Green, A. B. Watts, O. Davies, F. Chibesakunda, and R. Walker (2020), Tectonics and landscape of the Central African Plateau and their implications for a propagating Southwestern Rift in Africa, *Geochemistry, geophysics, geosystems: G(3)*, *21*, doi: 10.1029/2019GC008746.

Dauteuil, O., C. Picart, F. Guillocheau, M. Pickford, and B. Senut (2018), Cenozoic deformation and geomorphic evolution of the Sperrgebiet area (Southern Namibia), *Communications of the Geological Survey of Namibia*, *18*, 1–18.

Dauteuil, O., M. Jolivet, L. Gaudaré, and A.-M. Pastier (2023), Rainfall-induced ground deformation in southern Africa, *Terra nova*, *35*(4), 260–266, doi: 10.1111/ter.12650.

Dyer, H., D. Amitrano, and A.-B. Boullier (2012), Scaling properties of fault rocks, *Journal of structural geology*, *45*, 125–136.

Ellery, W., and T. McCarthy (1998), Environmental change over two decades since dredging and excavation of the lower Boro River, Okavango Delta, Botswana, *Journal of biogeography*, *25*(2), 361–378, doi: 10.1046/j.1365-2699.1998.252168.x.

Fernandes, R. M. S., J. M. Miranda, D. Delvaux, D. S. Stamps, and E. Saria (2013), Re-evaluation of the kinematics of Victoria Block using continuous GNSS data, *Geophysical journal international*, *193*(1), 1–10, doi: 10.1093/gji/ggs071.

Gaudaré, L., O. Dauteuil, and M. Jolivet (2024), Geomorphology of the Makgadikgadi Basin (Botswana): Insight into the propagation of the East African Rift System, *Tectonics*, *43*(2), e2023TC007,988, doi: 10.1029/2023tc007988.

Gratier, J.-P., F. Thouvenot, L. Jenatton, A. Tourette, M.-L. Doan, and F. Renard (2013), Geological control of the partitioning between seismic and aseismic sliding behaviours in active faults: Evidence from the Western Alps, France, *Tectonophysics*, *600*, 226–222.

Gumbricht, T., T. McCarthy, and C. L. Merry (2001), The topography of the Okavango Delta, Botswana, and its tectonic and sedimentological implications, *Suid-Afrikaanse tydskrif vir geologie [South African journal of geology]*, *104*(3), 243–264, doi: 10.2113/1040243.

Gumbricht, T., P. Wolski, P. Frost, and T. S. McCarthy (2004), Forecasting the spatial extent of the annual flood in the Okavango delta, Botswana, *Journal of Hydrology*, *290*(3-4), 178–191.

Haddon, I. G., and T. S. McCarthy (2005), The Mesozoic-Cenozoic interior sag basins of Central Africa: The Late Cretaceous-Cenozoic Kalahari and Okavango basins, *Journal of African Earth Sciences*, *43*, 316–333.

Huntsman-Mapila, P., S. Ringrose, A. Mackay, W. Downey, M. Modisi, S. Coetzee, J. Tiercelin, A. B. Kampunzu, and C. VanderPost (2006), Use of the geochemical and biological sedimentary record in establishing palaeo-environments and climate change in the Lake Ngami basin, NW Botswana, *Quaternary international: the journal of the International Union for Quaternary Research*, *148*(1), 51–64, doi: 10.1016/J.QUAINT.2005.11.029.

Jolivet, M., S. Arzhannikov, A. Chauvet, A. Arzhannikova, R. Vassallo, N. Kulagina, and V. Akulova (2013), commodating large-scale intracontinental extension and compression in a single stress-field: A key example from the Baikal Rift System, *Gondwana Research*, *24*, 918–935.

Jourdan, F., G. Féraud, H. Bertrand, A. B. Kampunzu, G. Tshoso, M. K. Watkeys, and B. Le Gall (2005), Karoo large igneous province: Brevity, origin, and relation to mass extinction questioned by new 40Ar/39Ar age data, *Geology*, *33*(9), 745–748, doi: 10.1130/G21632.1.

Junk, W. J., M. Brown, I. C. Campbell, M. Finlayson, B. Gopal, L. Ramberg, and B. G. Warner (2006), The comparative biodiversity of seven globally important wetlands: a synthesis, *Aquatic sciences*, *68*(3), 400–414, doi: 10.1007/s00027-006-0856-z.

Key, R., and N. Ayres (2000), The 1998 edition of the National Geological Map of Botswana, *Journal of African Earth Sciences*, *30*, 427–451, doi: 10.1016/S0899-5362(00)00030-0.

Kinabo, B. D., E. Atekwana, J. Hogan, M. Modisi, D. Wheaton, and A. B. Kampunzu (2007), Early structural development of the Okavango rift zone, NW Botswana, *Journal of African Earth Sciences*, *48*, 125–136, doi: 10.1016/J.JAFREARSCI.2007.02.005.

Landerer, F. W., and S. C. Swenson (2012), Accuracy of scaled GRACE terrestrial water storage estimates, *Water resources research*, *48*(W04531), 11, doi: 10.1029/2011WR011453.

Lovecchio, J. P., S. Rohais, P. Joseph, N. D. Bolatti, and V. A. Ramos (2020), Mesozoic rifting evolution of SW Gondwana: A poly-phased, subduction-related, extensional history responsible for basin formation along the Argentinean Atlantic margin, *Earth-science reviews*, *203*(103138), 103,138, doi: 10.1016/j.earscirev.2020.103138.

Materna, K., S. Wei, X. Wang, L. Heng, T. Wang, W. Chen, R. Salman, and R. Bürgmann (2019), Source characteristics of the 2017 Mw6.4 Moijabana, Botswana earthquake, a rare lower-crustal event within an ancient zone of weakness, *Earth and planetary science letters*, *506*, 348–359, doi: 10.1016/j.epsl.2018.11.007.

McCarthy, J. M., T. Gumbricht, T. McCarthy, P. Frost, K. Wessels, and F. Seidel (2003), Flooding patterns of the

Okavango wetland in Botswana between 1972 and 2000, *Ambio*, *32*(7), 453–457, doi: 10.1579/0044-7447-32.7.453.

McCarthy, T. S. (1993), The great inland deltas of Africa, *Journal of African earth sciences (and the Middle East)*, *17*(3), 275–291, doi: 10.1016/0899-5362(93)90073-y.

McCarthy, T. S. (2006), Groundwater in the wetlands of the Okavango Delta, Botswana, and its contribution to the structure and function of the ecosystem, *Journal of hydrology*, *320*(3-4), 264–282, doi: 10.1016/j.jhydrol.2005.07.045.

McCARTHY, T. S. (2013), The Okavango delta and its place in the geomorphological evolution of southern Africa, *Suid-Afrikaanse tydskrif vir geologie [South African journal of geology]*, *116*(1), 1–54, doi: 10.2113/gssajg.116.1.1.

McCarthy, T. S., R. W. Green, and N. J. Franey (1993), The influence of neo-tectonics on water dispersal in the northeastern regions of the Okavango swamps, Botswana, *Journal of African Earth Sciences*, *17*, 23–32.

McFarlane, M. J., and F. D. Eckardt (2006), Lake Deception: A New Makgadikgadi Palaeolake, *Botswana notes and records*, *38*, 195–201.

McFarlane, M. J., and P. Segadika (2001), Archaeological evidence for the reassessment of the ages of the Makgadikgadi paleolakes, *Botswana Notes & Records*, *33*(1), 83–90, doi: 10.10520/AJA052550590_115.

Mendelsohn, J., JM, C. Vanderpost, Ramberg, M. Murray-Hudson, P. Wolski, and K. Mosepele (2010), *Okavango Delta: Floods of Life*, RAISON (Research & Information Services of Namibia).

Miller, R. M. G. (2008), *The geology of Namibia: Archaean to mesoproterozoic*, Ministry of Mines and Energy Geological Survey of Namibia, Windhoek, Namibia.

Milzow, C., and W. Kinzelbach (2010), Accounting for subgrid scale topographic variations in flood propagation modeling using MODFLOW, *Water resources research*, *46*(10), doi: 10.1029/2009WR008088.

Milzow, C., L. Kgotlhang, P. Bauer-Gottwein, P. Meier, and W. Kinzelbach (2009), Regional review: the hydrology of the Okavango Delta, Botswana—processes, data and modelling, *Hydrogeology journal*, *17*(6), 1297–1328, doi: 10.1007/s10040-009-0436-0.

Mladenov, N., D. M. McKnight, P. Wolski, and M. Murray-Hudson (2007), Simulation of DOM fluxes in a seasonal floodplain of the Okavango Delta, Botswana, *Ecological modelling*, *205*(1-2), 181–195, doi: 10.1016/j.ecolmodel.2007.02.015.

Modisi, M. P. (2000), Fault system of the southeastern boundary of the Okavango Rift, Botswana, *Journal of African Earth Sciences*, *30*, 569–578.

Moliner Cachazo, L., K. Makati, M. A. Chadwick, J. A. Catford, B. W. Price, A. W. Mackay, M. D. Guiry, M. Murray-Hudson, and F. Murray-Hudson (2023), A review of the freshwater diversity in the Okavango Delta and Lake Ngami (Botswana): taxonomic composition, ecology, comparison with similar systems and conservation status, *Aquatic sciences*, *85*(4), 115, doi: 10.1007/s00027-023-01008-z.

Moore, A. E., F. P. D. Cotterill, and F. D. Eckardt (2012), The evolution and ages of makgadikgadi palaeo-lakes: Consilient evidence from Kalahari drainage evolution south-central Africa, *Suid-Afrikaanse tydskrif vir geologie [South African journal of geology]*, *115*(3), 385–413, doi: 10.2113/gssajg.115.3.385.

Murray-Hudson, M., P. Wolski, and S. Ringrose (2006), Scenarios of the impact of local and upstream changes in climate and water use on hydro-ecology in the Okavango Delta, Botswana, *Journal of hydrology*, *331*(1-2), 73–84, doi: 10.1016/j.jhydrol.2006.04.041.

Pastier, A.-M. (2018), The Okavango delta through the deformation of its surface : multi-proxy approach from hydrology to tectonics, Ph.D. thesis, Université de Rennes, Rennes, France.

Pastier, A.-M., O. Dauteuil, M. Murray-Hudson, F. Moreau, A. Walpersdorf, and K. Makati (2017), Is the Okavango Delta the terminus of the East African Rift System? Towards a new geodynamic model: Geodetic study and geophysical review, *Tectonophysics*, *712-713*(Supplement C), 469–481, doi: 10.1016/j.tecto.2017.05.035.

Podgorski, J. E., A. G. Green, L. Kgotlhang, W. K. H. Kinzelbach, T. Kalscheuer, E. Auken, and T. Ngwisanyi (2013), Paleo-megalake and paleo-megafan in southern Africa, *Geology*, *41*(11), 1155–1158, doi: 10.1130/G34735.1.

Podgorski, J. E., W. K. H. Kinzelbach, and L. Kgotlhang (2017), Using helicopter TEM to delineate fresh water and salt water zones in the aquifer beneath the Okavango Delta, Botswana, *Advances in water resources*, *107*, 265–279, doi: 10.1016/j.advwatres.2017.06.021.

Ramberg, L., P. Hancock, M. Lindholm, T. Meyer, S. Ringrose, J. Sliva, J. Van As, and C. Vander Post (2006), Species diversity of the Okavango delta, Botswana, *Aquatic sciences*, *68*(3), 310–337, doi: 10.1007/s00027-006-0857-y.

Ramsay, J. G., and M. I. Huber (1983), *The technique of modern structural geology. Volume 1: Strain Analysis*, Academis Press, London.

Ringrose, S., P. Huntsman-Mapila, A. Basira Kampunzu, W. Downey, S. Coetzee, B. Vink, W. Matheson, and C. Vanderpost (2005), Sedimentological and geochemical evidence for palaeo-environmental change in the Makgadikgadi subbasin, in relation to the MOZ rift depression, Botswana, *Palaeogeography, palaeoclimatology, palaeoecology*, *217*(3-4), 265–287.

Ringrose, S., P. Huntsman-Mapila, W. Downey, S. Coetzee, M. Fey, C. Vanderpost, B. Vink, T. Kemosidile, and D. Kolokose (2008), Diagenesis in Okavango fan and adjacent dune deposits with implications for the record of palaeo-environmental change in Makgadikgadi-Okavango-Zambezi basin, northern Botswana, *Geomorphology (Amsterdam, Netherlands)*, *101*(4), 544–557.

Saria, E., E. Calais, Z. Altamimi, P. Willis, and H. Farah (2013), A new velocity field for Africa from combined GPS and DORIS space geodetic Solutions: Contribution to the definition of the African reference frame (AFREF), *JOURNAL OF GEOPHYSICAL RESEARCH: SOLID EARTH*, *118*, 1–21.

Schmidt, G., F. Franchi, F. Salvini, A. T. Selepeng, E. Luzzi, C. Schmidt, and E. A. Atekwana (2023), Fault controlled geometries by inherited tectonic texture at the southern end of the East African Rift System in the Makgadikgadi Basin, northeastern Botswana, *Tectonophysics*, *846*(229678), 229,678, doi: 10.1016/j.tecto.2022.229678.

Shaw, P. (1984), A historical note on the outflows of the Okavango delta system, *Botswana Notes & Records*, *16*(1), 127–130, doi: 10.10520/aja052550590_748.

Stamps, D. S., E. Calais, E. Saria, C. Hartnady, J.-M. Nocquet,

C. J. Ebinger, and R. M. Fernandes (2008), A kinematic model for the East African Rift, *Geophysical research letters*, *35*(5), doi: 10.1029/2007GL032781.

Stamps, D. S., C. Kreemer, R. Fernandes, T. A. Rajaonarison, and G. Rambolamanana (2021), Redefining East African Rift System kinematics, *Geology*, *49*(2), 150–155, doi: 10.1130/g47985.1.

Takasu, T. (2010), Real-time PPP with RTKLIB and IGS real-time satellite orbit and clock, in *IGS Workshop*, Newcastle, England.

Thomas, D., and P. Shaw (1990), The deposition and development of the Kalahari Group sediments, Central Southern Africa, *Journal of African Earth Sciences*, *10*, 187–197, doi: 10.1016/0899-5362(90)90054-I.

Titus, S. J. (2006), Thirty-five-year creep rates for the creeping segment of the San Andreas fault and the effects of the 2004 Parkfield earthquake: Constraints from alignment arrays, continuous global positioning system, and creepmeters, *Bulletin of the Seismological Society of America*, *96*(4B), S250–S268, doi: 10.1785/0120050811.

Wanke, A., H. Stollhofen, I. G. Stanistreet, and V. Lorenz (2000), Karoo unconformities in NW-Namibia and their tectonic implications, *Communications of the Geological Survey of Namibia*, *12*, 259–268.

Wedmore, L. N. J., J. Biggs, M. Floyd, A. Fagereng, H. Mdala, P. Chindandali, J. N. Williams, and F. Mphepo (2021), Geodetic constraints on cratonic microplates and broad strain during rifting of thick southern African lithosphere, *Geophysical research letters*, *48*(17), doi: 10.1029/2021gl093785.

Wolski, P., and M. Murray-Hudson (2008), An investigation of permanent and transient changes in flood distribution and outflows in the Okavango Delta, Botswana, *Physics and Chemistry of the Earth*, *33*, 157–164.

Wolski, P., H. H. G. Savenije, M. Murray-Hudson, and T. Gumbricht (2006), Modelling of the flooding in the Okavango Delta, Botswana, using a hybrid reservoir-GIS model, *Journal of hydrology*, *331*(1-2), 58–72, doi: 10.1016/j.jhydrol.2006.04.040.

Wolski, P., M. Murray-Hudson, K. Thito, and L. Cassidy (2017), Keeping it simple: Monitoring flood extent in large data-poor wetlands using MODIS SWIR data, *International journal of applied earth observation and geoinformation: ITC journal*, *57*, 224–234, doi: 10.1016/j.jag.2017.01.005.

Wu, Y., Z. Jiang, G. Yang, W. Wei, and X. Liu (2011), Comparison of GPS strain rate computing methods and their reliability, *Geophysical journal international*, *185*(2), 703–717, doi: 10.1111/j.1365-246X.2011.04976.x.

Yu, Y., K. H. Liu, Z. Huang, D. Zhao, C. A. Reed, M. Moidaki, J. Lei, and S. S. Gao (2017), Mantle structure beneath the incipient Okavango rift zone in southern Africa, *Geosphere*, *13*(1), 102–111, doi: 10.1130/GES01331.1.